# BIOCHEMISTRY

including biophysical chemistry & molecular biology

Helix-Capping Histidines: Diversity of N−H⋯N Hydrogen Bond Strength Revealed by $^{2h}J_{NN}$ Scalar Couplings

Matthew R. Preimesberger,[†] Ananya Majumdar,[‡] Selena L. Rice,[†] Lauren Que,[†] and Juliette T. J. Lecomte*,[†]

[†]T. C. Jenkins Department of Biophysics, Johns Hopkins University, Baltimore, Maryland 21218, United States
[‡]Biomolecular NMR Center, Johns Hopkins University, Baltimore, Maryland 21218, United States

Ⓢ Supporting Information
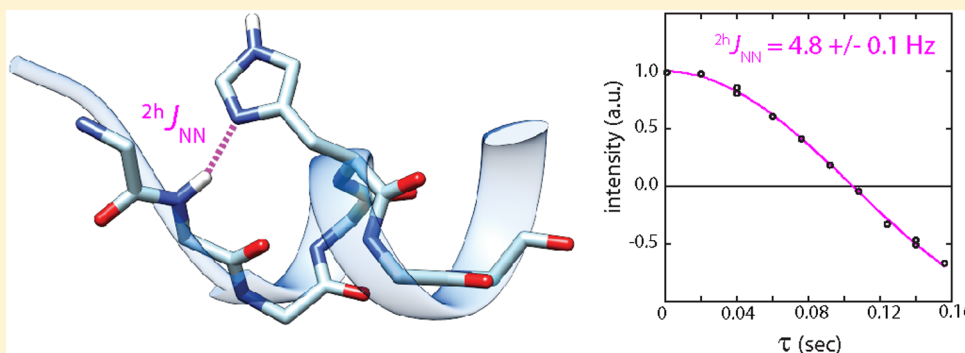
ABSTRACT: In addition to its well-known roles as an electrophile and general acid, the side chain of histidine often serves as a hydrogen bond (H-bond) acceptor. These H-bonds provide a convenient pH-dependent switch for local structure and functional motifs. In hundreds of instances, a histidine caps the N-terminus of α- and 3_{10}-helices by forming a backbone NH⋯Nδ1 H-bond. To characterize the resilience and dynamics of the histidine cap, we measured the *trans* H-bond scalar coupling constant, $^{2h}J_{NN}$, in several forms of Group 1 truncated hemoglobins and cytochrome b_5. The set of 19 measured $^{2h}J_{NN}$ values were between 4.0 and 5.4 Hz, generally smaller than in nucleic acids ($\sim$6−10 Hz) and indicative of longer, weaker bonds in the studied proteins. A positive linear correlation between $^{2h}J_{NN}$ and the difference in imidazole ring ^{15}N chemical shift ($\Delta^{15}N = |\delta^{15}N\delta1 - \delta^{15}N\varepsilon2|$) was found to be consistent with variable H-bond length and variable cap population related to the ionization of histidine in the capping and noncapping states. The relative ease of $^{2h}J_{NN}$ detection suggests that this parameter can become part of the standard arsenal for describing histidines in helix caps and other key structural and catalytic elements involving NH⋯N H-bonds. The combined nucleic acid and protein data extend the utility of $^{2h}J_{NN}$ as a sensitive marker of local structural, dynamic, and thermodynamic properties in biomolecules.

The importance of hydrogen bonds (H-bonds) in the folding and structural organization of biomacromolecules has been recognized for decades. "Hydrogen Bonding in Biological Structures"[1] presents an excellent historical perspective extending to the late 1980s. Since then, nuclear magnetic resonance (NMR) spectroscopy has emerged as an essential tool in the characterization of hydrogen bonding in both proteins and nucleic acids. Indeed, numerous NMR observables are available for assessing the presence, strength, and other fundamental characteristics of H-bonds. They include chemical shifts, fractionation factors, temperature coefficients, and hydrogen exchange rates. In favorable instances, these indirect manifestations can be complemented with direct detection of the H-bonding interaction. The parameter of interest in this work is the scalar coupling that connects NMR-active nuclei across the H-bond.[2−5] H-Bond scalar couplings (HBCs) have the advantage of identifying donor and acceptor atoms and are extraordinarily sensitive to geometric properties such as H-bond length.[5−8] In addition, because the magnitude of an HBC

is affected by time and ensemble averaging, HBCs can also inform on the local dynamics and energetics of H-bonds within biomacromolecules.[9−10]

The predominant H-bond of proteins is the backbone−backbone N−H⋯O=C′ sustaining regular secondary structure. The ^{15}N−^{13}C three-bond ($^{3h}J_{NC'}$) and ^1H−^{13}C two-bond ($^{2h}J_{HC'}$) couplings associated with these and similar interactions have been measured in several proteins under various conditions.[2,9,11−15] These couplings are invariably small (<1 Hz), which has focused application to diamagnetic proteins of fewer than 100 residues because of their favorable T_1 and T_2 relaxation times. In contrast, N−H⋯N H-bonds are relatively rare but exhibit ^{15}N−^{15}N two-bond couplings ($^{2h}J_{NN}$) between

2 and 11 Hz,[16−18] an experimentally accessible range for proteins with less-than-optimal relaxation properties.

Protein N−H···N H-bonds frequently involve a histidine as the acceptor and another histidine or a backbone amide as the donor. A perusal of X-ray structures suggests an average of one bond of the latter type in every three deposited structures and fewer yet of the side chain to side chain type. However, such rarity does not imply that protein N−H···N H-bonds are insignificant; participation in active sites and critical elements of structure, for example, N-terminal caps of helices,[19] along with unique ionization and tautomeric properties make histidines and their H-bonds especially interesting to study.

In its helix N-capping role, the histidine uses the $N\delta 1$ atom as an H-bond acceptor and adopts the $N\varepsilon 2$-H tautomeric state. Two capping configurations predominate, which we denote as i-to-i+3 and i-to-i−2, where i is the donor amide (Figure 1).
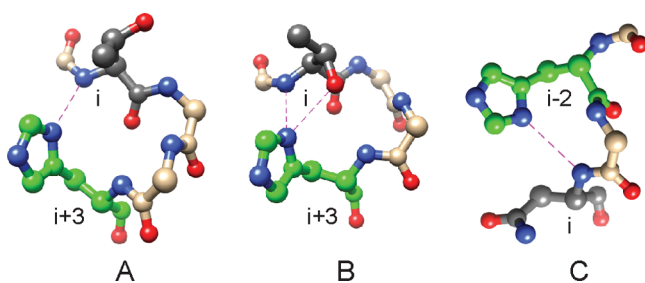

Figure 1. Helix capping by histidine. (A) i-to-i+3 N−H··$N\delta 1$ H-bond in *Synechococcus* GlbN (PDB entry 4MAX).[20] (B) Bifurcated i-to-i+3 N−H···$N\delta 1$···H−Oγ interaction in the consensus AR (PDB entry 2BKG).[21] (C) i-to-i−2 N−H···$N\delta 1$ H-bond in rat mitochondrial cytochrome b_5 (PDB entry 4HIL).

Recently, we have reported the detection of i-to-i+3 N−H···$N\delta 1$ H-bonds within the α-helix N-caps of ankyrin repeat (AR) proteins.[18] The consensus AR N-cap has the sequence TXXH

and is unusual in that the histidine $N\delta 1$ atom acts as a bifurcated H-bond acceptor to both threonine amide and hydroxyl hydrogens (Figure 1B) in an arrangement that conditions inter-repeat packing and the geometry of the first turn of helix. In the study presented here, we expanded the AR protein experiments to a greater set of histidine N-caps and chose those caps in heme proteins (truncated hemoglobins and cytochrome b_5) so that changes in heme placement, oxidation state, ligation state, or post-translational modification (PTM) could be exploited as perturbations to the N−H···$N\delta 1$ bond.

Truncated hemoglobins (TrHbs) share a basic architecture composed of seven helices labeled A−C and E−H by analogy to the canonical globins.[22] In one group of TrHbs (TrHb1s), α-helix G is initiated by a strong start signal[19] of the i-to-i+3 variety. The motif uses a histidine at the i+3 position in hundreds of TrHb1s, including those from the unicellular eukaryotes *Chlamydomonas eugametos* (CtrHb) and *Chlamydomonas reinhardtii* (THB1), and from the cyanobacteria *Synechocystis* sp. PCC 6803 (*Synechocystis* GlbN) and *Synechococcus* sp. PCC 7002 (*Synechococcus* GlbN). These homologous TrHb1s (~40−50% identical) differ in the sequence of the cap and the residues immediately preceding and following it. The TrHb1 cap is close to the heme group and on the same side as the "proximal" histidine (Figure S1A), a conserved ligand to the iron in the ferric (oxidized) and ferrous (reduced) states.

THB1 and both GlbNs are "hexacoordinate" hemoglobins. They ligate the heme iron with the proximal histidine and a distal lysine (THB1)[23] or histidine (GlbNs).[24,25] Exogenous ligands such as O_2 can displace the distal residue and force a conformational rearrangement bringing a tyrosine from the B helix (Tyr B10) and glutamine(s) from the E helix into the distal heme pocket.[20,23,26] The B and E helices affected by the ligand replacement are remote from the helix-capping H-bond (Figure S1A). Comparing HBCs with and without exogenous
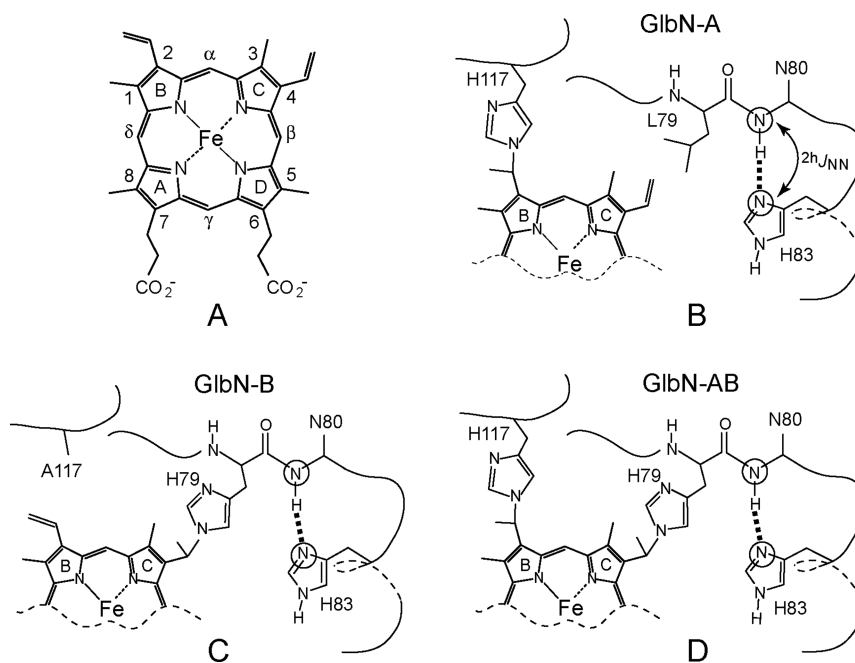

Figure 2. Heme b and its modifications in TrHb1s. (A) Heme b. (B) Native cross-link in wild-type *Synechococcus* and *Synechocystis* GlbN (GlbN-A). (C) Cross-link engineered in GlbN by placing a histidine at position 79 (GlbN-B). (D) Double cross-link engineered in GlbN (GlbN-AB). Amino acid labeling corresponds to that of *Synechocystis* GlbN.

ligand therefore offers an opportunity to assess long-range coupling between the distal and proximal sides of the heme.

In addition to hexacoordination, the two GlbNs have the ability to react with the heme group (Figure 2). The irreversible post-translational modification (PTM) involves His117, a noncoordinating histidine located on the H helix near the heme 2-vinyl group.[27] Heme reduction in the absence of oxygen causes spontaneous formation of the His117 Nε2−2-Cα heme linkage (Figure 2B)[28,29] and generates "GlbN-A". Recent work has demonstrated that analogous histidine−heme modifications can be engineered at the 4-vinyl group with the Leu79His replacement.[30] In the absence of the native (2-vinyl) cross-link, the 4-vinyl-reacted protein is denoted as GlbN-B (Figure 2C), whereas the doubly cross-linked material is termed GlbN-AB (Figure 2D). The "B" cross-link was also implanted into CtrHb with the Leu75His replacement (CtrHb-B).[31] Panels C and D of Figure 2 emphasize the proximity of the engineered modification to the α-helix N-cap. For our purposes, the artificial linkages serve to probe the response of the G helix N-cap to a nearby structural perturbation.

The i-to-$i-2$ motif often has a proline at the $i-1$ position and forms a tight turn adequate for capping 3_{10}-helices. This second type of N-capping N−H···Nδ1 H-bond is found in the electron transfer protein cytochrome b_5, where it initiates the C-terminal helix of the soluble heme domain. The H-bond is formed between His80 Nδ1 and Asp82 N−H and is more than 20 Å from the heme binding pocket (Figure S1B). The cap is preserved in the apoprotein,[32] although an ~1% capless population can be detected in the NMR data.[32,33] Figure 1C shows the structure of the 3_{10} histidine N-cap.

The goals of this work were 2-fold. First, we wanted to explore the use of $^{2h}J_{NN}$ as a semiquantitative reporter of stress in helix caps formed with a histidine side chain. The HBC values collected on TrHb1s and cytochrome b_5 in different states would inform on long-range transmission of perturbation. Second, we sought to add to the HBCs acquired on the helix caps of AR proteins[18] and compare the NMR properties of protein N−H···N H-bonds with those of nucleic acids.[3,34,35] These goals required the accurate measurement of $^{2h}J_{NN}$ HBCs in multiple proteins. As will be demonstrated, the data set uncovers trends in NMR parameters and extends the utility of $^{2h}J_{NN}$ HBCs for biophysical characterization in proteins. It also provides insights into the distinctive properties of HBCs involving an acceptor histidine.

■ MATERIALS AND METHODS

Protein Expression and Purification. Overexpression and purification of uniformly ^{15}N-labeled recombinant ferric TrHb1s and cytochrome b_5 were achieved as described previously.[23,25,36,37] A summary of the published procedures is provided in the Supporting Information. Covalently modified hemoglobins (GlbN-A, GlbN-B, GlbN-AB, and CtrHb-B) were produced by reduction of the ferric or cyanomet holoprotein with a 2−5-fold molar excess of dithionite (DT, >85%, Alfa-Aesar) for at least 15 min, followed by oxidation and purification.[30]

NMR Sample Preparation. Lyophilized ferric recombinant protein was dissolved in NMR buffer [0−125 mM sodium/potassium phosphate (pH 7.0−7.5) and 10% D$_2$O]. Cyanide-bound ferric hemoglobins were prepared by addition of a 2−5-fold molar excess of KCN (J. T. Baker). Ferrous cytochrome b_5 was produced by DT reduction of an ~3 mM ferric protein (1.5-fold molar excess of DT to protein) sample. To prevent

evaporation or oxidation, protein samples were transferred to Shigemi tubes and sealed with Parafilm M prior to the collection of NMR data. Protein concentrations ranged from 500 μM to 5 mM, although the concentrations of most samples were from ~1.0 to 2.5 mM. Under the chosen conditions, each protein is monomeric. Specific NMR sample conditions are listed in Table S1.

NMR Data Acquisition. NMR spectroscopy was conducted using 600.13 MHz Bruker Avance or 600.53 MHz Avance-II spectrometers, each equipped with a cryogenic probe. ^{1}H−^{15}N HSQC, histidine-selective ^{1}H−^{15}N long-range (LR) HMQC,[38] soft ^{1}H−(N)−^{15}N COSY,[39] and quantitative $^{2h}J_{NN}$ constant-time spin−echo (CTSE) difference 1D/2D HSQC spectra[39] were acquired as detailed elsewhere.[18] A typical $^{2h}J_{NN}$ CTSE series consisted of 12−20 1D or 2D spectra using different τ modulation periods and two or three duplicate values. For a representative 1−2 mM protein sample, a single $^{2h}J_{NN}$ CTSE 1D spectrum was acquired with 512−1024 transients, a constant-time relaxation delay of ~150 ms, and a recycle delay of ~1.0 s and therefore required ~10−20 min per data point. All ferric proteins in this study are paramagnetic ($S = \frac{1}{2}$). Unless otherwise noted, NMR data were collected at 313 K to improve H-bond detection. ^{1}H chemical shifts were referenced with respect to the water line (4.58 ppm at 313 K and 4.76 ppm at 298 K); ^{15}N chemical shifts were referenced indirectly using the Ξ ratio.[40]

NMR Data Processing, Analysis, and Curve Fitting. NMR data were processed with NMRPipe[41] or Topspin 2.1 (Bruker BioSpin). Spectra were analyzed using Sparky 3.[42] For $^{2h}J_{NN}$ modulation data, 1D peak intensities were obtained using the deconvolution (mixed Lorentzian/Gaussian) routine of Topspin 2.1. 2D peak volumes were calculated by peak integration (Sparky 3). Peak intensities were tabulated and plotted as a function of the $^{2h}J_{NN}$ modulation time, τ. The fit to the data was performed with Kaleidagraph (Synergy Software) and the equation $I(\tau) = A \cos(\pi J \tau)$ to extract the initial amplitude (A) and J coupling magnitude ($|^{2h}J_{NN}|$).[43] For some $^{2h}J_{NN}$ modulation curves, peak heights were substituted for intensities to yield better signal-to-noise ratios. However, the choice of heights or intensities did not significantly affect the best fit $^{2h}J_{NN}$ values. In most instances, the fitting error for $^{2h}J_{NN}$ was well below 0.1 Hz. The experimental error was based on peak intensities (or heights) in duplicate spectra collected at the beginning and end of an experimental series. The combined error estimate reported in Table 1 was typically <5%. The $^{2h}J_{NN}$ modulation curves plotted in Figure S3 have been normalized by their individually fitted amplitudes to facilitate comparison of peaks with different intensities.

Simulation of the pH Response. The influence of N−H···Nδ1 H-bonding on the histidine ionization equilibrium, observed $^{2h}J_{NN}$ couplings, and imidazole ^{15}N chemical shifts was explored using simulations performed with Scilab 5.4.1 (Scilab Entreprises S.A.S.). The thermodynamic model assumed the existence of four states: (1) a capped configuration in which the N−H···Nδ1 hydrogen bond is intact, coupling is active [$^{2h}J_{NN} = {}^{2h}J_{NN}$(capped)], and the histidine adopts the Nε2-H neutral tautomer, (2) an open state in which the hydrogen bond is broken ($^{2h}J_{NN} = 0$) and the histidine occurs as the Nε2-H neutral tautomer, (3) an open state in which the hydrogen bond is broken ($^{2h}J_{NN} = 0$) and the histidine occurs as the Nδ1-H neutral tautomer, and (4) an open imidazolium form ($^{2h}J_{NN} = 0$). The *cis* state of the cytochrome Xxx−Pro

Table 1. $^{2h}J_{NN}$ Values, Amide Donor ^{1}H Chemical Shifts, and Histidine ^{15}Nδ1 and ^{15}Nε2 Chemical Shifts Observed for N−H···Nδ1 Helix-Capping H-Bonds[a]

label[b]	protein	distal[c]	$\lvert^{2h}J_{NN}\rvert$ (Hz)	^{1}H (ppm)	δ^{15}Nε2 (ppm)	δ^{15}Nδ1 (ppm)
	CtrHb, M[d,e]	CN	5.3 ± 0.2	11.41	nd[f]	254.9
A	CtrHb, m[d]	CN	5.2 ± 0.2	11.39	166.6	254.9
B	CtrHb, M	CN	5.0 ± 0.1	11.17	166.5	255.1
C	CtrHb-B	CN	4.0 ± 0.3	10.45	168.6	249.6
D	THB1, M[g]	CN	4.8 ± 0.1	11.18	166.4	256.6
E	THB1, m[g]	CN	4.6 ± 0.3	11.28	166.9	256.9
F	Syn7002[h] GlbN	His	4.7 ± 0.2	10.77	166.9	256.4
G	Syn7002 GlbN-A	His	4.8 ± 0.2	10.97	167.3	256.6
H	Syn6803[i] GlbN[g]	CN	5.0 ± 0.2	11.34	165.9	257.7
I	Syn6803 GlbN-A[g]	CN	4.8 ± 0.2	11.40	166.1	258.0
J	Syn6803 GlbN	His	4.9 ± 0.2	11.14	165.8	257.4
K	Syn6803 GlbN-A	His	4.9 ± 0.2	11.28	166.0	257.5
L	Syn6803 GlbN-B	His	4.5 ± 0.2	10.93	166.9	255.3
M	Syn6803 GlbN-AB	His	4.3 ± 0.2	10.87	167.6	254.5
N	Syn6803 GlbN-B	CN	5.4 ± 0.1	11.40	166.0	256.9
O	Syn6803 GlbN-AB	CN	5.0 ± 0.1	11.29	166.4	257.1
P	ferric cyt b_5	His	5.0 ± 0.1	10.88	165.0	250.5
Q	ferrous cyt b_5	His	5.0 ± 0.1	10.94	165.3	250.6
R	apocyt b_5[j]	–	5.3 ± 0.1	11.15	165.0	250.3

[a]Measured at 313 K, 10% D_2O, and pH 7.0−7.2 on proteins containing ferric heme iron unless otherwise noted. [b]As annotated in Figure 5. [c]Distal ligand to the heme iron. [d]M, major heme isomer; m, minor heme isomer. [e]Measured at 283 K. [f]Not determined. [g]Measured at pH 7.3−7.5. [h]Syn7002, Synechococcus sp. PCC 7002. [i]Syn6803, Synechocystis sp. PCC 6803. [j]Measured at 298 K.

bond was not detected, and the Xxx−Pro *cis*−*trans* equilibrium was not considered in the modeling.

The input parameters included the microscopic pK_a for the capped state and both open states. For the open state, we chose the values of Nα-acetyl-histidine methylamide to eliminate terminal charge and intramolecular H-bonding effects.[44] As determined by Tanokura,[45] the imidazolium form dissociates to the Nε2H tautomer (open, Nε2H) with a pK_a of 6.53 and to the Nδ1H tautomer (open, Nδ1H) with a pK_a of 6.92. The Hill coefficients (n_H) characterizing proton uptake[46] were all held at unity. The fractional populations of the four forms (capped, Nε2H; open, Nε2H; open, Nδ1H; and open, +) were evaluated as a function of pH using eqs 1−5.

$$F(\text{capped, N}\varepsilon 2\text{H}) = 10^{\text{pH}-\text{p}K_a(\text{capped})}/Q \tag{1}$$

$$F(\text{open, N}\varepsilon 2\text{H}) = 10^{\text{pH}-6.53}/Q \tag{2}$$

$$F(\text{open, N}\delta 1\text{H}) = 10^{\text{pH}-6.92}/Q \tag{3}$$

$$F(\text{open, +}) = 1/Q \tag{4}$$

$$Q = 1 + 10^{\text{pH}-\text{p}K_a(\text{capped})} + 10^{\text{pH}-6.92} + 10^{\text{pH}-6.53} \tag{5}$$

where Q is the partition function using the open protonated state as the reference. The predicted histidine ^{15}N chemical shifts were calculated assuming fast exchange on the ^{15}N chemical shift time scale using eqs 6 and 7:

$$
\begin{aligned}
^{15}\text{N}\varepsilon 2(\text{observed}) = {} & 165 \times F(\text{capped, N}\varepsilon 2\text{H}) \\
& + 167.5 \times F(\text{open, N}\varepsilon 2\text{H}) \\
& + 266.5 \times F(\text{open, N}\delta 1\text{H}) \\
& + 176.5 \times F(\text{open, +}) \tag{6}
\end{aligned}
$$

$$
\begin{aligned}
^{15}\text{N}\delta 1(\text{observed}) = {} & 258 \times F(\text{capped, N}\varepsilon 2\text{H}) \\
& + 261.5 \times F(\text{open, N}\varepsilon 2\text{H}) \\
& + 183.5 \times F(\text{open, N}\delta 1\text{H}) \\
& + 176.5 \times F(\text{open, +}) \tag{7}
\end{aligned}
$$

The coefficients in eqs 6 and 7 correspond to the limiting ^{15}N chemical shift values of Vila (neutral open tautomers)[47] and Pelton and co-workers (imidazolium);[38] the limiting ^{15}N chemical shift values for the "capped, Nε2H" state were chosen to encompass the experimentally determined heme protein ^{15}N chemical shifts. We note that the open state pK_as were determined at 310 K.[45] No correction was applied to these values when considering experimental data at 313 K. Open state pK_as at 298 K were adjusted assuming a histidine enthalpy of ionization of +30 kJ/mol.[48]

Database Analysis. The structures of proteins determined by X-ray crystallography with better than 1.5 Å resolution were collected from the Protein Data Bank (July 30, 2015) and culled at 70% identity. Each of the 3253 structures was examined for the presence of amide−histidine N−Nδ1 pairs having an interatomic distance of <3.2 Å. Hydrogens were ignored, and a small number of structures having short N−Cδ2 distances were not assessed for the plausibility of alternative histidine χ^2 angles. A representative set of helix caps (one chain per structure) was extracted from the data to obtain inter-nitrogen distance distributions for the two types of caps. The histogram in Figure 11 was optimized for bin size with a published method.[49] In addition, 77 myoglobin structures (resolution better than 1.5 Å) containing the His24−His119 pair were collected and the Nε2−Nε2 distances measured for comparison with the N-capping H-bonds.

■ RESULTS

N−H···N H-Bonding in Cyanomet CtrHb. We first present the data collected with one of the globins, namely CtrHb, in the ferric state with cyanide as the distal ligand [cyanomet CtrHb, or CtrHb-CN (PDB entry 1DLY)].[50] The putative *i*-to-*i*+3 interaction in CtrHb involves Ser76 and His79 and is a convenient subject for illustrating the spectroscopic manifestations of the capping H-bonds along with the utility of solution phase characterization. The nuclei of interest are the backbone amide ^{15}N and ^{1}H nuclei and the histidine ^{15}Nδ1, ^{1}Hε1, ^{15}Nε2, and ^{1}Hδ2 nuclei. These are the targets of *J*-correlated experiments designed to establish unambiguously the existence of the N−H···Nδ1 H-bond.

The amide ^{1}H−^{15}N HSQC spectrum of CtrHb-CN shows two sets of cross-peaks (Figure 3A) corresponding to two heme orientations in the heme pocket. The major and minor isomers, related by an ∼180° rotation of the heme about its α−γ meso axis, are in slow exchange on the chemical shift time scale and occur in a 7:3 ratio in this protein.[31] Sequence specific assignments identify the amide proton signals of Ser76 at
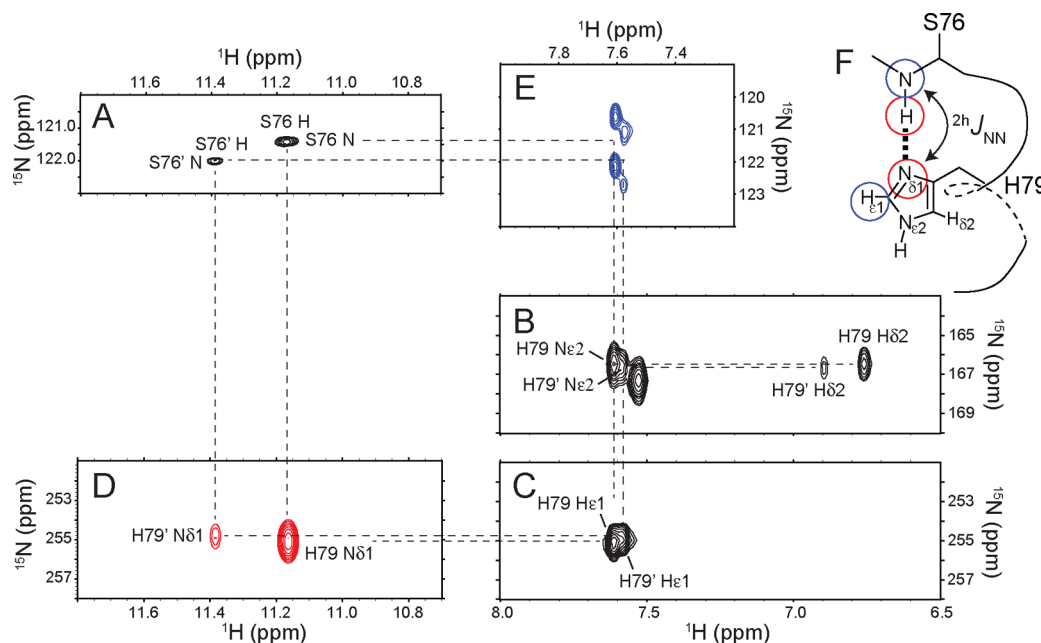
Figure 3. Identification of the N−H···Nδ1 H-bond in CtrHb-CN. (A) ^{1}H−^{15}N HSQC (downfield amide ^{1}H region). The minor heme isomer is denoted with a prime. (B) ^{1}H−^{15}N LR-HMQC (upfield ^{15}N region). (C) ^{1}H−^{15}N LR-HMQC (downfield ^{15}N region). (D) ^{1}H−(N)−^{15}Nδ1 COSY. (E) ^{1}H-coupled ^{1}Hε1−(Nδ1)−^{15}N−(H) LR-COSY. (F) Ser76 N−H···Nδ1 His79 helix-capping scheme in *C. eugametos* CtrHb-CN. Correlated nuclei determined by the NMR data shown in panels D and E are highlighted with red and blue circles, respectively.

downfield shifts of ~11.2 ppm (major isomer) and ~11.4 ppm (minor isomer). Notably, high-resolution HSQC data show that both Ser76 cross-peaks appear as 5 Hz doublets in the ^{15}N dimension (Figure S2A,B), a fine structure that is absent from all other ^{15}N−^{1}H cross-peaks.

Histidine-selective ^{1}H−^{15}N LR-HMQC spectra obtained with CtrHb-CN were analyzed in previous work.[31] They show that major His79 and minor His79 are deprotonated at neutral pH, adopt the Nε2H tautomer, and have Nδ1 signals at ~255 ppm (Figure 3B,C and Table 1). Backbone amide ^{1}H−^{15}N HSQC spectra acquired with ^{15}N decoupling centered at the His79 Nδ1 frequency during the evolution period contain collapsed Ser76 doublets (Figure S2C). This observation is in agreement with a ~ 5 Hz $^{2h}J_{NN}$ caused by the Ser76−His79 H-bond. In addition, a weak cross peak between His79 ^{15}Nδ1 and the amide proton of Ser76 (major isomer) is detected in the high sensitivity ^{1}H−^{15}N LR-HMQC data (Figure S2D,E). Because these *J*-correlated nuclei are separated by 14 covalent bonds, the observed connectivity must arise via the one-bond *trans* HBC, $^{1h}J_{HN}$.

To document further the presence of the N−H···Nδ1 H-bond, a soft ^{1}H−(N)−^{15}N COSY experiment[18,39] was used. Unlike the LR-HMQC, the HNN-COSY pulse sequence utilizes the two-bond homonuclear HBC $^{2h}J_{NN}$ for N−H···N H-bond identification. This approach is advantageous because the $^{2h}J_{NN}$ coupling is often considerably larger than the $^{1h}J_{HN}$ coupling[4] and therefore leads to a gain in sensitivity. Figure 3D illustrates the results of such an experiment. Two peaks are present in the spectrum and identify Ser76 amide ^{1}H and His79 ^{15}Nδ1 within the N−H···N H-bonds (major and minor isomers). In agreement, the ^{1}H-coupled ^{1}H−(N)−^{15}N−(H) LR COSY data[51] shown in Figure 3E also display two $^{2h}J_{NN}$-mediated peaks and correlate His79 ^{1}Hε1 with Ser76 ^{15}N, the latter split by its directly attached proton ($|^1J_{NH}| \sim 90$ Hz). The NMR connectivity pattern shown in Figure 3 is unequivocal

evidence of the N−H···Nδ1 H-bond between Ser76 and His79 in CtrHb-CN.

To determine if the $^{2h}J_{NN}$ coupling constants involving a histidine ring may be practical reporters for H-bond properties, we measured the magnitude of the $^{2h}J_{NN}$ couplings using a high-precision quantitative CTSE difference HSQC experiment.[43] With this method, amide NH groups within N−H···Nδ1 H-bonds undergo $^{2h}J_{NN}$ modulation according to the timing (τ) of a histidine-selective ^{15}Nδ1 inversion pulse. Repeating the experiment for different values of τ yields a modulation curve from which the magnitude of $^{2h}J_{NN}$ can be accurately extracted. Figure 4A presents the downfield region of 1D data collected for CtrHb-CN. The intensities of the resolved Ser76 NH protons were plotted as a function of the $^{2h}J_{NN}$ modulation time τ and fit according to the relationship $I(\tau) = A \cos(\pi J \tau)$.[43]

The data in Figure 4B yield a well-defined value ($|^{2h}J_{NN}| = 5.0 \pm 0.1$ Hz, major isomer) for the Ser76−His79 N−H···Nδ1 interaction, in agreement with the directly observed splitting (Figure S2A,B). The minor heme isomer has the same coupling constant within error $[|^{2h}J_{NN}| = 5.2 \pm 0.2$ Hz (Figure S3A)]. Decreasing the temperature from 313 to 283 K yielded a relatively constant $|^{2h}J_{NN}|$ $[5.3 \pm 0.2$ Hz, major isomer (Figure S3S)]. The magnitude of the CtrHb-CN $^{2h}J_{NN}$ couplings is within the range expected from the few previously reported instances of amide N−H···N His H-bonds (~2−6 Hz).[16,18]

N−H···N H-Bonding in THB1-CN and *Synechocystis* GlbN-CN. We collected HSQC, LR-HMQC, HNN-COSY, and $^{2h}J_{NN}$ CTSE difference spectra to characterize the N−H···N H-bonds in THB1-CN (Asn87−His90) and *Synechocystis* GlbN-CN (Asn80−His83). These proteins yielded HNN-COSY signals (Figure 5) and $^{2h}J_{NN}$ values (Table 1 and Figure S3D,E,H) similar to those of CtrHb-CN, in a suggestion that sequence context and the identity of the amide donor (Ser in CtrHb and Asn in *Synechocystis* GlbN and THB1) have minimal effects on the helix-capping H-bond. GlbN-CN with native heme PTM (GlbN-A-CN) yielded a $^{2h}J_{NN}$ value $[4.8 \pm 0.2$ Hz
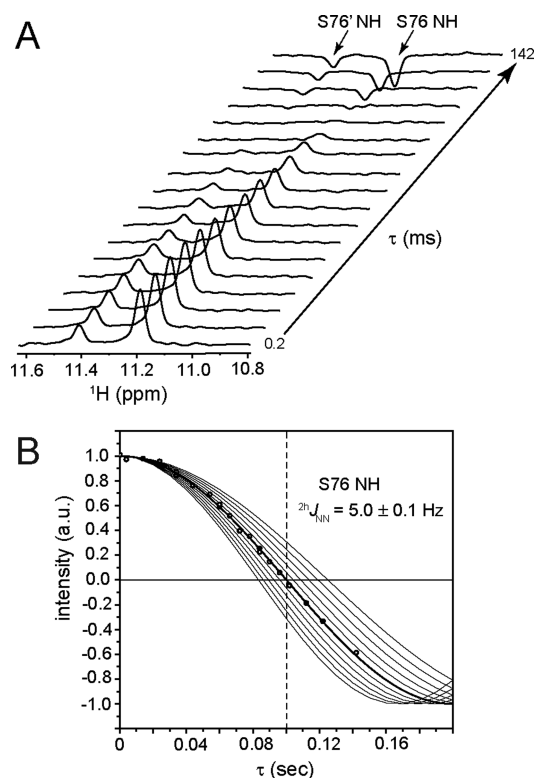
Figure 4. Measurement of the $^{2h}J_{NN}$ magnitude in CtrHb-CN. (A) Stack plot showing the resolved amide proton resonances of Ser76 (major and minor isomers) as a function of the $^{2h}J_{NN}$ modulation time, τ. (B) Normalized Ser76 NH peak intensities (major isomer, black circles) as a function of τ. The horizontal black line indicates zero intensity, and the black dashed vertical line corresponds to the null time for $^{2h}J_{NN}$ = 5 Hz (100 ms). Simulated $^{2h}J_{NN}$ curves (black lines) between 4 and 6 Hz in 0.2 Hz increments are included for comparison.
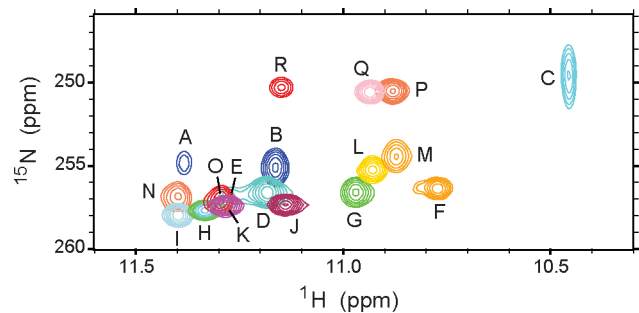
Figure 5. Overlay of HNN-COSY spectra. Data collected on hemoglobins and holocytochrome b_5 at 313 K and apocytochrome b_5 at 298 K (peak R). Each cross-peak corresponds to the amide ^{1}H and His ^{15}Nδ1 of an N−H···Nδ1 H-bond, correlated by $^{2h}J_{NN}$. The peak labels are defined in the first column of Table 1.

(Figure S3I)] close to that in its unmodified form. Thus, the native His117−2-Cα cross-link appears to have little influence on the N−H···Nδ1 H-bond in the cyanomet complexes.

N−H···N H-Bonding in Bis-histidine *Synechocystis* and *Synechococcus* GlbNs. To examine how binding of cyanide to the distal heme site and the consequent conformational rearrangement alter the N−H···N N-cap, we prepared *Synechococcus* and *Synechocystis* GlbNs with and without PTM in their ferric bis-histidine state. All four species yielded observable HNN-COSY cross-peaks (Figure 5) and $^{2h}J_{NN}$ values of 4.7−4.9 Hz (Table 1 and Figure S3F,G,J,K). These results indicate insensitivity to the distal ligand and associated structural differences in the wild-type GlbNs, regardless of heme modification status. In the case of *Synechococcus* GlbN, which contains a TXXH motif as in the previously studied AR proteins,[18] no evidence of bifurcated N−H···Nδ1···H−Oγ H-bonding was observed. In addition, the relatively constant magnitude of $^{2h}J_{NN}$ detected for wild-type TrHb1s from *C. eugametos*, *C. reinhardtii*, *Synechococcus*, and *Synechocystis* (4.6−5.2 Hz) was greater than the $^{2h}J_{NN}$ values obtained for the bifurcated H-bonds of ARs (1.8−4.1 Hz),[18] in support of a shorter N···Nδ1 distance in the former proteins.

Influence of Engineered His-Heme PTM on the Helix-Capping N−H···N H-Bond. Non-native heme modifications can be introduced into *Synechocystis* GlbN as depicted in panels C and D of Figure 2. *Synechocystis* GlbN-B and GlbN-AB exhibit bis-histidine coordination as in the wild-type protein.[30] Figure 5 shows the correlations between Asn80 backbone amide ^{1}H and His83 ^{15}Nδ1 and therefore the presence of the helix-capping N−H···N H-bonds. However, the data demonstrate systematic upfield shifts for Asn80 ^{1}H and His83 ^{15}Nδ1 nuclei relative to GlbN-A. Measurement of the $^{2h}J_{NN}$ couplings (Table 1 and Figure S3L,M) also suggests H-bond lengthening (or weakening) relative to the bis-histidine wild-type reference.

Upon replacement of the distal histidine with cyanide in GlbN-B and GlbN-AB, the H-bonds persist (Figure 5). In contrast to observations in the bis-histidine state, Asn80 ^{1}H and His83 ^{15}Nδ1 resonances have large downfield shifts. Furthermore, a significant (∼16−20%) increase in the $^{2h}J_{NN}$ coupling constants is measured in both GlbN-AB-CN (+0.7 Hz; $^{2h}J_{NN}$ = 5.0 Hz) and GlbN-B-CN (+0.9 Hz; $^{2h}J_{NN}$ = 5.4 Hz) (Table 1 and Figure S3O,N). This is presumably due to H-bond relaxation relative to the strained bis-histidine complexes. Thus, formation of the engineered linkage to the FG turn, adjacent to the helix N-cap, couples distal cyanide binding to the proximal side of the heme pocket in a manner not observed in the wild-type proteins.

A non-native histidine−heme covalent modification analogous to that in *Synechocystis* GlbN-B can be engineered in CtrHb.[31] HNN-COSY (Figure 5) and $^{2h}J_{NN}$ modulation experiments performed with CtrHb-B-CN (Figure S3C) demonstrate that the N−H···Nδ1 H-bond is considerably perturbed ($^{2h}J_{NN}$ = 4.0 Hz) relative to its wild-type reference [$^{2h}J_{NN}$ = 5.0 Hz (Table 1)]. These results suggest that the formation of the engineered cross-link to the FG turn in CtrHb-B-CN generates strain in the adjacent helix-capping H-bond. The ∼20% decrease in $^{2h}J_{NN}$ observed for CtrHb-B-CN compared to wild-type CtrHb-CN is in contrast to that of the GlbN-B-CN and GlbN-CN pair [8% increase by cross-linking (Table 1)]. The opposite effect of the engineered cross-link in CtrHb-CN and GlbN-CN on the G helix N-cap implicates a difference in the conformational plasticity of neighboring elements of structure. It is worth noting that the F-helix/FG loop sequence preceding the cap in CtrHb (VPHL) is shorter by two residues than in GlbN (VENHGL).

N−H···N H-Bonding in the His-Pro-Asp Motif of Cytochrome b_5. To study the *i*-to-*i*−2 motif and its response to iron redox changes and heme binding, we prepared the ferric, ferrous, and apoprotein states of cytochrome b_5. As in the hemoglobins, the N−H donor proton resonates downfield from its random shift (HSQC data on the ferric form shown in Figure S4A). Also in agreement with previous work,[36] histidine-selective LR-HMQC spectra confirm that His80 is neutral and that its Nδ1 atom is deprotonated (Figure S4B). HNN-COSY

data recorded for the ferric protein (Figure S4C), the ferrous protein, and the apoprotein (Figure 5) support the presence of the N−H···Nδ1 H-bond (Figure 1C) in all three forms of the cytochrome. Measurement of $^{2h}J_{NN}$ returned values of 5.0, 5.0, and 5.3 Hz for the ferric form (313 K), ferrous form (313 K), and apoprotein form (298 K, for stability reasons), respectively (Table 1 and Figure S3P−R). Thus, the His-Pro-Asp N−H···N H-bond of cytochrome b_5 depends little on the iron redox state or the presence of the heme. Additionally, the cytochrome b_5 i-to-i−2 H-bond appears to be similar to those detected within the TrHb1 i-to-i+3 motifs.

■ DISCUSSION

N−H···N H-Bonding, $^{2h}J_{NN}$, and Histidine pK_a. The $^{2h}J_{NN}$ data obtained with the hemoglobins and cytochrome suggest that this parameter can register long-range influences and be a reliable indicator of the state of an N-capping H-bond. However, to interpret the $^{2h}J_{NN}$ values, it is essential to consider that the observables may be ensemble averages over the H-bonded state having a limiting $^{2h}J_{NN}$ equal to $^{2h}J_{NN}$(capped) and one or more nonbonded states having a $^{2h}J_{NN}$ equal to 0. We will assume that nonbonded states expose the histidine to solvent, in which case there are three possible open species: the imidazolium (protonated) state, the Nε2-H tautomer (imidazolium pK_a ∼ 6.53), and the Nδ1-H tautomer (imidazolium pK_a ∼ 6.92).[44,45,52] The two tautomers partition in an ∼5:2 ratio dictated by the pK_a values. The set of relevant equilibria is presented in Figure 6. Although the details of this scheme are expected to differ from protein to protein and conditions to conditions, the thermodynamic analysis provides a framework with which to scrutinize the significance of the $^{2h}J_{NN}$ measurements.

To perform the simulation shown in Figure 7A, the microscopic pK_a of the histidine in the H-bonded state was set to 4, 5, or 6. For each pK_a value, the fractional population of all four states was calculated as a function of pH using eqs 1−5. As the histidine pK_a in the capped state approaches that of the open state, the maximal attainable fraction of the H-bonded form drops below 1. Under such conditions, the observed $^{2h}J_{NN}$ value does not reach $^{2h}J_{NN}$(capped) and the observed histidine chemical shifts do not correspond to the pure state limiting chemical shifts. Capping histidine pK_as have been published[32,36,53] or were estimated in this work (Figures S6−S8 and Table S2); they suggest that in most cases, the pK_a is sufficiently low (<4.5) that a direct measurement of $^{2h}J_{NN}$(capped) is possible. Open/closed averaging may be influential for the solvent-exposed cap of AR proteins,[18] CtrHb-B-CN, and cytochrome b_5, and in those instances, extrapolation of the observed $^{2h}J_{NN}$ is necessary to estimate $^{2h}J_{NN}$(capped). In this framework, $^{2h}J_{NN}$(capped) is a parameter determined primarily by bond length,[54] and K_{close} (Figure 6) is a measure of bond strength directly related to the free energy of H-bond formation, $\Delta G_f°$.[55]

For the i-to-i+3 N−H···N N-cap of consensus AR proteins, we found that buried H-bonds have larger observed couplings ($^{2h}J_{NN}$ ∼ 4−5 Hz) than H-bonds exposed to solvent ($^{2h}J_{NN}$ ∼ 2 Hz). We also note that H-bonds with larger $^{2h}J_{NN}$ values are exhibited by histidines having a depressed ionization constant (pK_a < 3), whereas those with smaller values have an only moderately depressed pK_a (∼5.7). Assuming a macroscopic pK_a of 5.7 (Figure S6), a simulation similar to that shown in Figure 7 leads to a closed state population of 77% at the pH of the AR
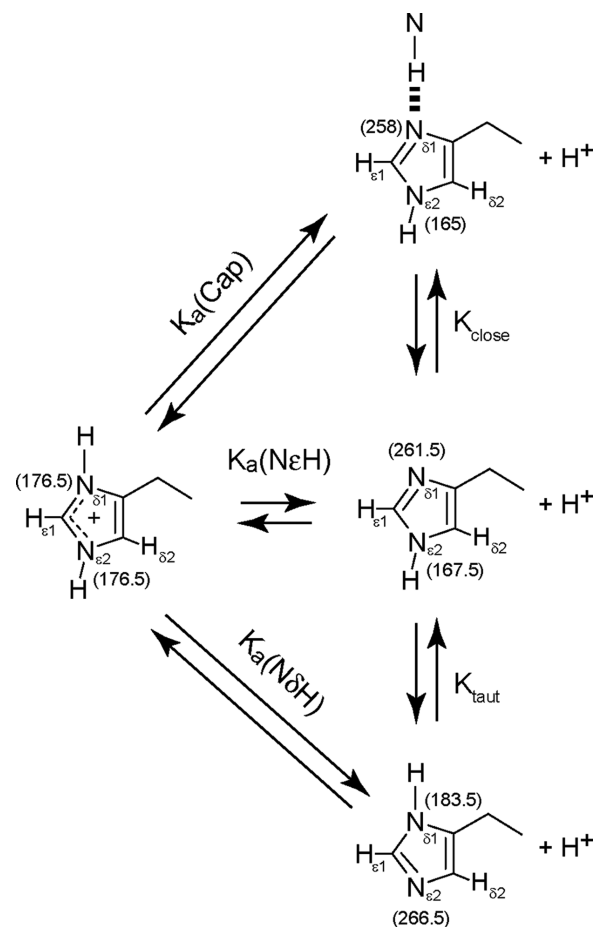

Figure 6. Scheme used to assess the effect of fast exchange averaging on histidine−amide H-bonding and histidine ^{15}N chemical shifts. The histidine can adopt an H-bonded state in which $^{2h}J_{NN}$ is active. The open states are characterized by a $^{2h}J_{NN}$ of 0 and partition according to sample pH and microscopic pK_a values. Limiting ^{15}Nδ1 and ^{15}Nε2 chemical shifts[38,47] are listed in parentheses. The limiting ^{15}N chemical shifts for the H-bonded state are estimates based on globins with large Δ^{15}N values and low apparent histidine pK_a values.

$^{2h}J_{NN}$ measurement (6.6). The model indicates that increasing the pH by one unit leads to a closed state population of 86% and an increase in $^{2h}J_{NN}$ (+0.23 Hz), in good agreement with pH-dependent NMR data (Figure S6). Extrapolation to a vanishing population of open states predicts a $^{2h}J_{NN}$(capped) of ∼2.7 Hz for the solvent-exposed H-bond, which can be meaningfully compared to the $^{2h}J_{NN}$(capped) of buried H-bonds [where $^{2h}J_{NN}$ ∼ $^{2h}J_{NN}$(capped) ∼ 4 Hz].

The same analysis was applied to CtrHb-CN. NMR data demonstrate that His79 in WT CtrHb-CN remains neutral until global acid unfolding, suggesting a pK_a of <3.5 (Figure S7A,B). In contrast, His79 in L75H CtrHb-B-CN undergoes partial protonation at pH 5.5 in support of a pK_a near 5 (Figure S7C,D). Thus, at pH 7.2, the wild-type N−H···Nδ1 H-bond is formed ∼100% of the time and the L75H variant H-bond only ∼95% of the time. A hypothetical fully formed H-bond in L75H CtrHb-B-CN would therefore give rise to a $^{2h}J_{NN}$(capped) value of ∼4.2 Hz, lower than the wild-type value of 5.0 Hz. The parameters used in the simulations are listed in Table S3.

In both examples, the low $^{2h}J_{NN}$(capped) and low observed $^{2h}J_{NN}$ values are likely manifestations of H-bond lengthening

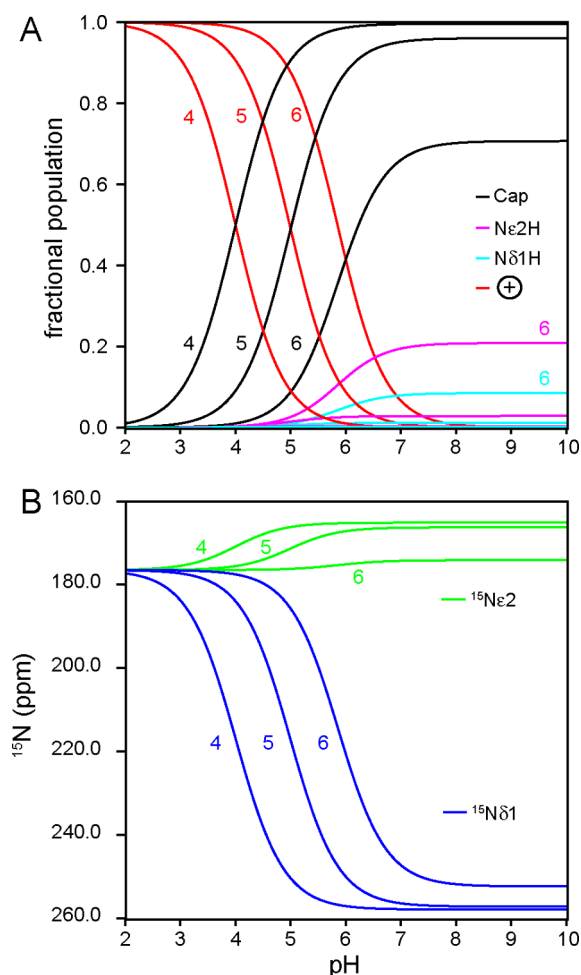**Figure 7.** Effect of capping histidine pK_a on (A) microstate fractional populations and (B) histidine $^{15}N\delta1$ and $^{15}N\varepsilon2$ chemical shifts. Fast exchange averaging among imidazolium (red trace), capped $N\varepsilon2$-H (black trace), and open $N\delta1$-H and $N\varepsilon2$-H histidine tautomers (cyan and magenta traces, respectively) was assumed. In panel B, the limiting ^{15}N chemical shift values were as defined in Figure 6. In both simulations, the capping histidine pK_a was set to 4, 5, or 6 as indicated on the traces. As the capping histidine pK_a nears the model compound values, a significant proportion of open states persists at neutral and higher pH, which reduces the maximal observable $\Delta^{15}N$.

and concomitant increased sampling of open states, respectively. The contribution from open/closed averaging is also possible in cytochrome b_5. When the estimated apoprotein pK_as of the H-bonded ($\sim$5.0)[36] and open ($\sim$6.9)[32] states were used in the simulation, $^{2h}J_{NN}$(capped) was evaluated at $\sim$5.5 Hz. In general, the modeling can be adjusted to account for deviations of the open state pK_a from the fully exposed residue and guide the choice of experimental conditions under which a satisfactory estimate of $^{2h}J_{NN}$(capped) can be obtained.

Fast Exchange Averaging and $^{2h}J_{NN}$–Chemical Shift Correlations. Histidine nitrogen shifts have been the subject of multiple studies. ^{14}N NMR studies of azoles[56] and extension to ^{15}N NMR of free histidine in solution,[44] model imidazoles,[57] and histidine within the catalytic triad of α-lytic protease[58] define the ring nitrogens as one of two types: the pyrrole α-type, which is protonated and has an upfield ^{15}N shift (167.5 ppm in imidazole and 176.5 ppm in imidazolium),[38] and the pyridine β-type, which is deprotonated and resonates downfield (^{15}N = 249.5 ppm).[38] The canonical limiting values for neutral

histidine were recently revised with density functional theory (DFT) calculations,[47] which return shifts of 167.5 ppm (Nε2) and 261.5 ppm (Nδ1) for the Nε2-H tautomer and shifts of 183.5 ppm (Nδ1) and 266.5 ppm (Nε2) for the Nδ1-H tautomer (Figure 6). According to the revised values, the theoretical maximal separation between the Nδ1 and Nε2 signals ($\Delta^{15}N = |\delta^{15}N\delta1 - \delta^{15}N\varepsilon2|$) is 94 ppm for the N$\varepsilon$2-H tautomer and 83 ppm for the Nδ1-H tautomer.

Under fast exchange on the chemical shift time scale, the ^{15}N chemical shifts of the neutral ring reflect the $\sim$5:2 Nε2-H:Nδ1-H ratio, and $\Delta^{15}N$ is smaller than for the pure tautomeric states. As the pH is lowered, protonation of the ring occurs, which changes the β-nitrogen to an α-like nitrogen and also reduces $\Delta^{15}N$. The N-capping interaction favors the Nε2-H tautomer and contributes primarily to a large $\Delta^{15}N$, but secondarily, H-bonding tends to shift the acceptor Nδ1 β-type nitrogen upfield of its maximal value,[59] thereby leading to a small reduction in $\Delta^{15}N$. These competing influences and local context typically render histidine ^{15}N chemical shifts difficult to interpret.

A plot of $^{2h}J_{NN}$ versus $\Delta^{15}N$ is shown in Figure 8 for the globins, cytochrome b_5, and AR proteins. The observed ^{15}N separations are below the DFT-derived maximum value of 94 ppm.
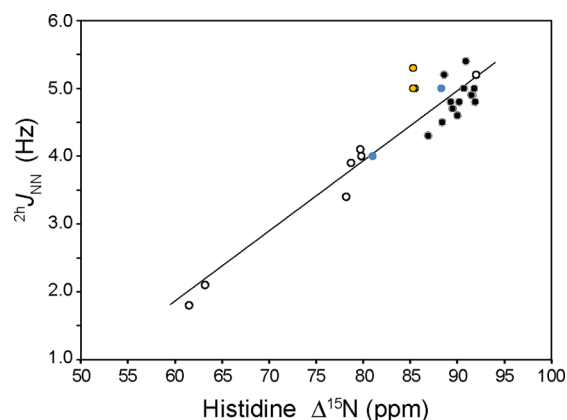

Figure 8. Plot of $^{2h}J_{NN}$ vs histidine $\Delta^{15}N$ for globins (black fill), cytochrome b_5 (orange fill), and AR proteins (O). Data for WT CtrHb-CN (for the major isomer, $^{2h}J_{NN}$ = 5.0 Hz and $\Delta^{15}N$ = 88.3 ppm) and L75H CtrHb-B-CN ($^{2h}J_{NN}$ = 4.0 Hz, and $\Delta^{15}N$ = 81 ppm) are colored blue. Linear regression of the full data set returns a slope of 0.10 Hz/ppm and an x-intercept ($\Delta^{15}N$ for $^{2h}J_{NN}$ = 0 Hz) of 43.3 ppm (r^2 = 0.88). Linear regression of the AR protein data alone yields a slope of 0.11 Hz/ppm and an x-intercept of 45.4 ppm (r^2 = 0.98), whereas the heme protein data alone (omitting apo cytochrome b_5) return a slope of 0.06 Hz/ppm and an x-intercept of 10.5 ppm (r^2 = 0.29).

Although significant scatter is present in the heme protein data, the composite $\Delta^{15}N$ values are positively correlated to $^{2h}J_{NN}$ such that larger couplings are associated with larger $\Delta^{15}N$. This behavior is characterized by large variations in the acceptor ($^{15}N\delta1$) chemical shift [larger coupling, larger shift (Table 1)]. The other ring nitrogen ($^{15}N\varepsilon2H$) displays modest variations that are negatively correlated to $^{2h}J_{NN}$ (larger coupling, smaller shift). The AR protein data span the greatest range of $^{2h}J_{NN}$ (1.8−5.2 Hz), $\Delta^{15}N$ (61.5−92.0 ppm), and pK_a (<3.0−5.7) values; in addition, their $^{2h}J_{NN}$ versus $\Delta^{15}N$ correlation is the strongest. In contrast, the heme protein data cluster around similar $^{2h}J_{NN}$ (4.0−5.4 Hz), $\Delta^{15}N$ (81.0−

91.9 ppm), and pK_a (<4.0−5.0) values and show only a weak positive correlation between $^{2h}J_{NN}$ and $\Delta^{15}N$.

The positive correlation between the histidine Nδ1 chemical shift and $^{2h}J_{NN}$ is noteworthy. For a pyridine β-type acceptor that is H-bonded 100% of the time, as H-bond length decreases, we expect the magnitude of $^{2h}J_{NN}$ to increase and the ^{15}Nδ1 shift to decrease (i.e., move upfield) as the nitrogen nucleus assumes greater α character.[8] The reverse trend is observed. To determine if open/closed averaging may be responsible, we simulated the pH profile of the ^{15}N chemical shifts as a function of histidine pK_a predicted by the model shown in Figure 6. The imidazole ^{15}N shifts, calculated with eqs 6 and 7, are presented in Figure 7B. Interestingly, the model predicts a linear relationship between $\Delta^{15}N$ and the fractional population of the capped form; thus, a linear correlation between $\Delta^{15}N$ and the magnitude of $^{2h}J_{NN}$ may also be expected. Assuming pH 7.2 and $^{2h}J_{NN}$(capped) = 5 Hz, the model predicts a 0.09 Hz/ppm line with an x-intercept ($\Delta^{15}N$ for $^{2h}J_{NN}$ = 0 Hz) of 37 ppm, values similar to those obtained from linear regression of the experimental data (Figure 8).

The $^{2h}J_{NN}$ values and chemical shifts for heme proteins (Table 1) and AR proteins[18] were combined in a plot of $^{2h}J_{NN}$ coupling versus amide ^{1}H chemical shifts (Figure 9). In this
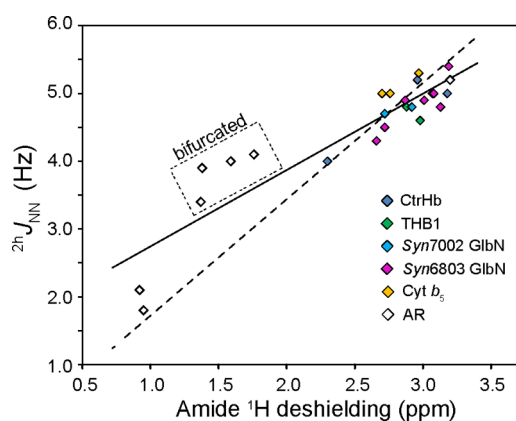

Figure 9. Plot of $^{2h}J_{NN}$ vs the amide ^{1}H-corrected chemical shift in heme proteins (fill colors correspond to Figure S5) and AR proteins ($\diamond$).[18] Linear regression of the entire data set gives a slope of 1.13 Hz/ppm and a y-intercept of 1.62 Hz [r^2 = 0.84 (—)]. The non-zero y-intercept is attributed to the lack of data at low J values. Fixing the y-intercept to zero yields a best fit slope of 1.72 Hz/ppm [r^2 = 0.59 (−−−)]. Linear regression of the heme protein data alone returns a slope of 1.13 Hz/ppm and a y-intercept of 1.56 Hz [r^2 = 0.55 (not shown)].

plot, the shifts were corrected for random coil values and the effect of nearest neighbors in the primary structure.[60] Paramagnetic effects, though estimated to be small at the cap site (~0.2 ppm), are likely to contribute to the scatter of the heme protein data along with secondary and tertiary structure differences. Despite this referencing problem, a positive correlation emerges by which greater ^{1}H deshielding accompanies greater $^{2h}J_{NN}$ coupling, as anticipated.[61]

The chemical shift trend in Figure 9 is reminiscent of the trend observed for Hoogsteen and Watson−Crick base pairs in triplex DNA[34] and prompts a comparison of the new protein data to published nucleic acid information. In nucleic acids, $^{2h}J_{NN}$ has been especially useful for inspecting the diversity of H-bond geometries. For example, ultra-high-resolution crystallographic structures of model U-A and G-C base pairs

support the possibility that the former have slightly shorter N−N H-bonding distances ($\Delta d \sim 0.05$ Å).[62,63] In agreement, the central imino N1−H···N3 H-bond within an RNA G-C base pair typically displays $^{2h}J_{NN}$ values between 5 and 7 Hz, on average smaller than those of the imino N3−H···N1 H-bond found in RNA (DNA) U-A (T-A) pairs (6−8 Hz).[3,4,64] Similarly, cooperative networks of amino N2−H···N7 H-bonds found in G-quadruplex DNA display $^{2h}J_{NN}$ values of 6−8 Hz.[35] Hoogsteen C-G base pairs involving protonated cytidine contain short, electrostatically stabilized H-bonds (N3$^+$−H···N7) and display the largest $^{2h}J_{NN}$ values yet measured in a biomacromolecule (10−11 Hz).[34] On the other hand, A-A mismatches, which have amino N6−H···N7-type H-bonds, tend to display low $^{2h}J_{NN}$ values (2−3 Hz), in support of their nonideal geometry.[39] In addition, a positive correlation between the imino donor ^{1}H chemical shift and the magnitude of $^{2h}J_{NN}$, which encompasses C$^+$(N3)−G(N7), T(N3)−A(N1), T(N3)−A(N7), and G(N1)−C(N3) bond types within triplex DNA, has been reported.[34] Similar observations have been made between the amide donor ^{1}H shift and |$^{3h}J_{NC'}$| within N−H···O=C′ protein H-bonds.[11]

The parallel between protein and nucleic acid N−H···N data is apparent in a plot of $^{2h}J_{NN}$ couplings versus raw ^{1}H shifts (Figure 10). The different absolute magnitude of protein
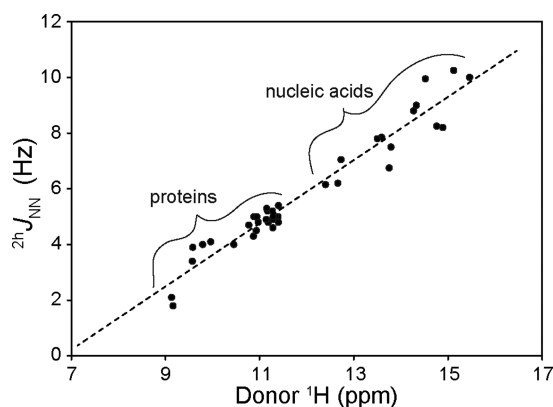

Figure 10. Plot of $^{2h}J_{NN}$ vs donor ^{1}H chemical shift for globin and cytochrome b_5 (this work), AR protein,[18] and nucleic acid[34] N−H···N H-bonds. A linear regression of the combined data returns a slope of 1.13 Hz/ppm and an x-intercept (^{1}H chemical shift for $^{2h}J_{NN}$ = 0) of 6.83 ppm (r^2 = 0.94).

and nucleic acid $^{2h}J_{NN}$ values supports the idea that in solution, both Watson−Crick and Hoogsteen N−H···N H-bonds in the DNA triplex are shorter (and possibly stronger) than the helix-capping amide N−H···Nδ1 His H-bond in proteins. This observation may reflect the fact that the difference in pK_a between the donor and acceptor groups in the nucleic acids is significantly smaller than that of an amide−histidine pair.[7,65] The analysis of combined raw protein amide and nucleic acid imino ^{1}H chemical shifts is particularly susceptible to the referencing problem mentioned above, but remarkably, the aggregate data describe a relatively constant slope and consistent linear behavior.

$^{2h}J_{NN}$ and Internuclear Distance. As per Figure 7, capping histidines with a pK_a near or below 4 and open state pK_as close to model compound values are expected to have a neutral-pH $^{2h}J_{NN}$ equal to $^{2h}J_{NN}$(capped) and be directly related to the geometry of the H-bond. Del Bene and co-workers have demonstrated that the coupling originates principally from the

Fermi contact interaction and that, accounting for differences in equilibrium bond length, the coupling is not particularly sensitive to the hybridization or charge state of the donor and acceptor groups.[6,7,54] The inter-nitrogen distance is the main determinant of the coupling magnitude, with angular dependence becoming steep only at large deviations from ideal geometry. The distance dependence is captured by an exponential decay[7] that can be used to rationalize our results. Figure 11 places the estimated $^{2h}J_{NN}$(capped) in this context.

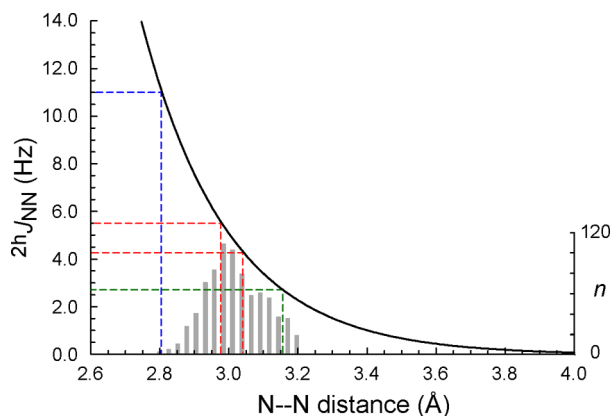**Figure 11.** Dependence of $^{2h}J_{NN}$(capped) on inter-nitrogen distance as approximated by the Fermi contact contribution to coupling.[7] The equation is $^{2h}J_{NN}$ (Hz) = 795579 exp(−3.9868 d), where d is the inter-nitrogen distance in angstroms.[7] The red dashed lines bracket the values measured in this work. The green dashed line indicates the $^{2h}J_{NN}$(capped) predicted for the solvent-exposed cap of AR proteins. The blue dashed line indicates the value reported for the His24−His119 pair of apomyoglobin.[17] The optimized histogram[49] (right ordinate) is for 803 nonredundant i-to-i−2 and i-to-i+3 distances of <3.2 Å obtained from the PDB survey.

The range covered by the hemoglobin and cytochrome values is framed by red dotted lines; the corresponding N−N atomic separations are between ∼2.98 and 3.04 Å. The lowest predicted $^{2h}J_{NN}$(capped) of 2.7 Hz is associated with a separation of 3.16 Å.

The accuracy of J-derived distances can be cross-validated with a survey of N-capping characteristics in available protein crystallographic structures. For the i-to-i−2 H-bonds with an intervening Pro, the mean inter-nitrogen distance is 3.00 ± 0.08 Å (n = 298). For the i-to-i+3 H-bonds, the distribution has a similar mean of 3.00 ± 0.09 Å (n = 70). These values are in good agreement with the predicted distances obtained from our solution $^{2h}J_{NN}$ data. Interestingly, the His−His Nε2-H···Nε2 bond in apomyglobin has a significantly larger $^{2h}J_{NN}$ (∼11 Hz).[17] Inspection of multiple holomyoglobin structures reveals a short inter-nitrogen distance [2.77 ± 0.10 Å (n = 77)]. The histidine pair has the same properties in apo- and holomyoglobin (buried, low acceptor pK_a),[66] and it is therefore reasonable to expect that the H-bond characteristics are maintained. Again using the Fermi contact curve of Figure 11,[7] a remarkable correspondence between the measured J and N−N distance is obtained (blue dashed line).

It is difficult to associate a free energy with the variation in $^{2h}J_{NN}$ detected here, in part because of uncertainty in the determination of K_{close} in Figure 6. However, the work of Del Bene suggests that in the relevant range of distances, a 1 Hz difference in $^{2h}J_{NN}$(capped) corresponds to several kilojoules per mole in binding energy.[54] In agreement, the 2 unit increase

in histidine pK_a for CtrHb-B compared to that of CtrHb (Figure S7) corresponds to a 100-fold change in K_{close} (assuming a common model pK_a for the open states) and gives rise to a 0.8 Hz difference in $^{2h}J_{NN}$(capped). Thus, qualitatively, the perturbations caused by heme modification do appear to have a significant local effect on H-bond geometry and, consequently, on the open/closed equilibrium of the helix cap. A full quantitative analysis would require knowledge of the pH dependence of protein stability and measurement of the histidine "open" state pK_as.

■ CONCLUSION

In this work, we demonstrated that helix-capping N−H···N H-bonds can be routinely detected in ^{15}N-labeled proteins using hydrogen bond scalar coupling experiments. Direct assignment of H-bonding nuclei was achieved by tailoring HNN-COSY and CTSE difference experiments for protein amide ^{15}N−^{1}H and histidine ^{15}Nδ1 nuclei. Evaluation of the $^{2h}J_{NN}$ coupling constants, along with knowledge of the histidine pK_a, provides a convenient metric for the length and relative strength of N−H···N H-bonds. In addition, a linear correlation between $^{2h}J_{NN}$ couplings and donor ^{1}H chemical shift emerges as observed for N−H···N H-bonds in Watson−Crick and Hoogsteen DNA base pairs. The absolute magnitude of the protein couplings tends to be smaller than those in nucleic acids and hints that in solution, DNA/RNA N−H···N H-bond lengths are likely shorter (∼2.8−2.9 Å) than those in the studied proteins (∼3.0−3.1 Å). Other varieties of N−H···N H-bonds, for example, those using tryptophan as a donor or deprotonated lysine as an acceptor, are feasible as well. Indeed, the LR-HNN-COSY experiments[51] (Figure 3E) could be used to overcome instances in which rapid hydrogen exchange precludes detection of the shared proton.

The open/closed capping model (Figure 6) suggests that longer, weaker H-bonds will lead to decreased $^{2h}J_{NN}$ (and decreased amide ^{1}H and imidazole Δ^{15}N chemical shifts) through two primary mechanisms: (1) increased N−N distance leading to decreased n → σ* donation and weaker Fermi contact interaction and (2) enhanced sampling of the open non-H-bonded states (each with $^{2h}J_{NN}$ = 0). Thus, only for strong H-bonds [∼100% closed, where $^{2h}J_{NN}$ = $^{2h}J_{NN}$(capped)] can the relative magnitude of $^{2h}J_{NN}$ be interpreted purely in terms of H-bond geometry. For weaker H-bonds, the expected distance and angular dependencies are obscured; specifically, open/closed averaging will always lead to a decrease in the observed $^{2h}J_{NN}$ value and therefore a population-dependent overestimate of H-bond length.

We envision that $^{2h}J_{NN}$ measurements can be routinely extended to resolve persistent questions of enzyme mechanism. Perturbation of individual H-bonds could be probed in the presence or absence of inhibitors, within a series of homologous enzymes or variants, and under different environmental conditions. The sensitivity of $^{2h}J_{NN}$ to bonding geometry and time-averaged population could reveal information not otherwise accessible by other solution methods or inspection of crystallographic structures. Several proteins for which NMR data have been published can be used as examples. (1) His95, in the active site of triosephosphate isomerase (PDB entry 1TIM),[67] has a depressed pK_a that allows this residue to be an efficient electrophile over a broad pH range.[68] H-Bond formation with the backbone amide of Glu97 is thought to be responsible at least in part for the low pK_a.[68,69] (2) Likewise, His187, in the active site of uracil DNA glycosylase, functions

in the neutral state, and its low pK_a is attributed to a capping interaction.[70,71] (3) In E2 ligases, the histidine of the conserved His-Pro-Asn motif has been proposed to play a catalytic role, but there is also support for a strictly structural role (histidine locked in the cap position).[72] (4) Tautomeric state switching in the dual-histidine motif of peptidyl prolyl isomerase has been proposed as an integral feature of the allosteric mechanism.[73] In each of these instances, measurements of $^{2h}J_{NN}$ HBCs would settle controversies or provide a robust indicator of H-bond presence and strength in the solution state.

ASSOCIATED CONTENT

Supporting Information

The Supporting Information is available free of charge on the ACS Publications website at DOI: 10.1021/acs.bio-chem.5b01002.

Details of protein preparation, NMR experiment conditions, simulation details, additional spectra, J modulation curves, and pH titrations (three tables and eight figures) (PDF)

AUTHOR INFORMATION

Corresponding Author

*E-mail: lecomte_jtj@jhu.edu. Telephone: (410) 516-7019.

Notes

The authors declare no competing financial interest.

ACKNOWLEDGMENTS

ABBREVIATIONS

1D, one-dimensional; 2D, two-dimensional; AR, ankyrin repeat; CtrHb, heme domain of *C. eugametos* LI637 hemoglobin; CtrHb-B, CtrHb with heme covalently attached to the FG turn; CTSE, constant-time spin−echo; DT, sodium dithionite; GlbN, *Synechocystis* or *Synechococcus* hemoglobin; GlbN-A, GlbN with heme covalently attached to the H helix; GlbN-AB, GlbN with heme covalently attached to the FG turn and H helix; GlbN-B, GlbN with heme covalently attached to the FG turn; H-bond, hydrogen bond; HBC, hydrogen bond scalar coupling; $^nJ_{xy}$, scalar coupling between nuclei x and y separated by n bonds; $^{2h}J_{NN}$, two-bond N−N HBC; LR, long-range; Mb, myoglobin; PDB, Protein Data Bank; PTM, post-translational modification; THB1, hemoglobin 1 from *C. reinhardtii*; TrHb1, Group 1 truncated hemoglobin.

REFERENCES

(1) Jeffrey, G. A., and Saenger, W. (1994) *Hydrogen Bonding in Biological Structures*, Springer, New York.

(2) Cornilescu, G., Hu, J. S., and Bax, A. (1999) Identification of the hydrogen bonding network in a protein by scalar couplings. *J. Am. Chem. Soc. 121*, 2949−2950.

(3) Dingley, A. J., and Grzesiek, S. (1998) Direct observation of hydrogen bonds in nucleic acid base pairs by internucleotide $^2J_{NN}$ couplings. *J. Am. Chem. Soc. 120*, 8293−8297.

(4) Pervushin, K., Ono, A., Fernandez, C., Szyperski, T., Kainosho, M., and Wüthrich, K. (1998) NMR scalar couplings across Watson-Crick base pair hydrogen bonds in DNA observed by transverse relaxation optimized spectroscopy. *Proc. Natl. Acad. Sci. U. S. A. 95*, 14147−14151.

(5) Dingley, A. J., Cordier, F., and Grzesiek, S. (2001) An introduction to hydrogen bond scalar couplings. *Concepts Magn. Reson. 13*, 103−127.

(6) Del Bene, J. E., Perera, S. A., and Bartlett, R. J. (2001) $^{15}N,^{15}N$ spin-spin coupling constants across N-H-N and N-H+-N hydrogen bonds: can coupling constants provide reliable estimates of N-N distances in biomolecules? *Magn. Reson. Chem. 39*, S109−S114.

(7) Del Bene, J. E., and Elguero, J. (2006) Systematic ab initio study of ^{15}N-^{15}N and ^{15}N-^1H spin-spin coupling constants across N-H+-N hydrogen bonds: Predicting N-N and N-H coupling constants and relating them to hydrogen bond type. *J. Phys. Chem. A 110*, 7496−7502.

(8) Barfield, M., Dingley, A. J., Feigon, J., and Grzesiek, S. (2001) A DFT study of the interresidue dependencies of scalar J-coupling and magnetic shielding in the hydrogen-bonding regions of a DNA triplex. *J. Am. Chem. Soc. 123*, 4014−4022.

(9) Jaravine, V. A., Alexandrescu, A. T., and Grzesiek, S. (2001) Observation of the closing of individual hydrogen bonds during TFE-induced helix formation in a peptide. *Protein Sci. 10*, 943−950.

(10) Luy, B., and Marino, J. P. (2000) Direct evidence for Watson-Crick base pairs in a dynamic region of RNA structure. *J. Am. Chem. Soc. 122*, 8095−8096.

(11) Cordier, F., and Grzesiek, S. (1999) Direct observation of hydrogen bonds in proteins by interresidue $^{3h}J_{NC'}$ scalar couplings. *J. Am. Chem. Soc. 121*, 1601−1602.

(12) Cordier, F., and Grzesiek, S. (2004) Quantitative comparison of the hydrogen bond network of A-state and native ubiquitin by hydrogen bond scalar couplings. *Biochemistry 43*, 11295−11301.

(13) Liu, A. Z., Hu, W. D., Majumdar, A., Rosen, M. K., and Patel, D. J. (2000) NMR detection of side chain-side chain hydrogen bonding interactions in $^{13}C/^{15}N$-labeled proteins. *J. Biomol. NMR 17*, 305−310.

(14) Cordier, F., Wang, C., Grzesiek, S., and Nicholson, L. K. (2000) Ligand-induced strain in hydrogen bonds of the c-Src SH3 domain detected by NMR. *J. Mol. Biol. 304*, 497−505.

(15) Cordier, F., Rogowski, M., Grzesiek, S., and Bax, A. (1999) Observation of through-hydrogen-bond $^{2h}J_{HC'}$ in a perdeuterated protein. *J. Magn. Reson. 140*, 510−512.

(16) Eletsky, A., Heinz, T., Moreira, O., Kienhofer, A., Hilvert, D., and Pervushin, K. (2002) Direct NMR observation and DFT calculations of a hydrogen bond at the active site of a 44 kDa enzyme. *J. Biomol. NMR 24*, 31−39.

(17) Hennig, M., and Geierstanger, B. H. (1999) Direct detection of a histidine-histidine side chain hydrogen bond important for folding of apomyoglobin. *J. Am. Chem. Soc. 121*, 5123−5126.

(18) Preimesberger, M. R., Majumdar, A., Aksel, T., Sforza, K., Lectka, T., Barrick, D., and Lecomte, J. T. J. (2015) Direct NMR detection of bifurcated hydrogen bonding in the α-helix N-caps of ankyrin repeat proteins. *J. Am. Chem. Soc. 137*, 1008−1011.

(19) Aurora, R., and Rose, G. D. (1998) Helix capping. *Protein Sci. 7*, 21−38.

(20) Wenke, B. B., Lecomte, J. T. J., Heroux, A., and Schlessman, J. L. (2014) The 2/2 hemoglobin from the cyanobacterium *Synechococcus* sp. PCC 7002 with covalently attached heme: comparison of X-ray and NMR structures. *Proteins: Struct., Funct., Genet. 82*, 528−534.

(21) Binz, H. K., Kohl, A., Pluckthun, A., and Grutter, M. G. (2006) Crystal structure of a consensus-designed ankyrin repeat protein: implications for stability. *Proteins: Struct., Funct., Genet. 65*, 280−284.

(22) Perutz, M. F. (1979) Regulation of oxygen affinity of hemoglobin: influence of structure of the globin on the heme iron. *Annu. Rev. Biochem. 48*, 327−386.

(23) Johnson, E. A., Rice, S. L., Preimesberger, M. R., Nye, D. B., Gilevicius, L., Wenke, B. B., Brown, J. M., Witman, G. B., and Lecomte, J. T. J. (2014) Characterization of THB1, a *Chlamydomonas reinhardtii* truncated hemoglobin: linkage to nitrogen metabolism and identi-

fication of lysine as the distal heme ligand. *Biochemistry* 53, 4573−4589.

(24) Couture, M., Das, T. K., Savard, P. Y., Ouellet, Y., Wittenberg, J. B., Wittenberg, B. A., Rousseau, D. L., and Guertin, M. (2000) Structural investigations of the hemoglobin of the cyanobacterium *Synechocystis* PCC 6803 reveal a unique distal heme pocket. *Eur. J. Biochem.* 267, 4770−4780.

(25) Scott, N. L., Falzone, C. J., Vuletich, D. A., Zhao, J., Bryant, D. A., and Lecomte, J. T. J. (2002) The hemoglobin of the cyanobacterium *Synechococcus* sp. PCC 7002: Evidence for hexacoordination and covalent adduct formation in the ferric recombinant protein. *Biochemistry* 41, 6902−6910.

(26) Trent, J. T., 3rd, Kundu, S., Hoy, J. A., and Hargrove, M. S. (2004) Crystallographic analysis of *Synechocystis* cyanoglobin reveals the structural changes accompanying ligand binding in a hexacoordinate hemoglobin. *J. Mol. Biol.* 341, 1097−1108.

(27) Vu, B. C., Jones, A. D., and Lecomte, J. T. J. (2002) Novel histidine-heme covalent linkage in a hemoglobin. *J. Am. Chem. Soc.* 124, 8544−8545.

(28) Nothnagel, H. J., Preimesberger, M. R., Pond, M. P., Winer, B. Y., Adney, E. M., and Lecomte, J. T. J. (2011) Chemical reactivity of *Synechococcus* sp. PCC 7002 and *Synechocystis* sp. PCC 6803 hemoglobins: covalent heme attachment and bishistidine coordination. *JBIC, J. Biol. Inorg. Chem.* 16, 539−552.

(29) Preimesberger, M. R., Pond, M. P., Majumdar, A., and Lecomte, J. T. J. (2012) Electron self-exchange and self-amplified posttranslational modification in the hemoglobins from *Synechocystis* sp. PCC 6803 and *Synechococcus* sp. PCC 7002. *JBIC, J. Biol. Inorg. Chem.* 17, 599−609.

(30) Preimesberger, M. R., Wenke, B. B., Gilevicius, L., Pond, M. P., and Lecomte, J. T. J. (2013) Facile heme vinyl posttranslational modification in a hemoglobin. *Biochemistry* 52, 3478−3488.

(31) Rice, S. L., Preimesberger, M. R., Johnson, E. A., and Lecomte, J. T. J. (2014) Introduction of a covalent histidine-heme linkage in a hemoglobin: A promising tool for heme protein engineering. *J. Inorg. Biochem.* 141, 198−207.

(32) Lecomte, J. T. J., and Moore, C. D. (1991) Helix formation in apocytochrome b_5: the role of a neutral histidine at the N-cap position. *J. Am. Chem. Soc.* 113, 9663−9665.

(33) Davis, R. B., Jr., and Lecomte, J. T. J. (2006) A dynamic N-capping motif in cytochrome b_5: evidence for a pH-controlled conformational switch. *Proteins: Struct., Funct., Genet.* 63, 336−348.

(34) Dingley, A. J., Masse, J. E., Peterson, R. D., Barfield, M., Feigon, J., and Grzesiek, S. (1999) Internucleotide scalar couplings across hydrogen bonds in Watson-Crick and Hoogsteen base pairs of a DNA triplex. *J. Am. Chem. Soc.* 121, 6019−6027.

(35) Dingley, A. J., Peterson, R. D., Grzesiek, S., and Feigon, J. (2005) Characterization of the cation and temperature dependence of DNA quadruplex hydrogen bond properties using high-resolution NMR. *J. Am. Chem. Soc.* 127, 14466−14472.

(36) Moore, C. D., al-Misky, O. N., and Lecomte, J. T. J. (1991) Similarities in structure between holocytochrome b_5 and apocytochrome b_5: NMR studies of the histidine residues. *Biochemistry* 30, 8357−8365.

(37) Scott, N. L., and Lecomte, J. T. J. (2000) Cloning, expression, purification, and preliminary characterization of a putative hemoglobin from the cyanobacterium *Synechocystis* sp. PCC 6803. *Protein Sci.* 9, 587−597.

(38) Pelton, J. G., Torchia, D. A., Meadow, N. D., and Roseman, S. (1993) Tautomeric states of the active-site histidines of phosphorylated and unphosphorylated IIIGlc, a signal-transducing protein from *Escherichia coli*, using two-dimensional heteronuclear NMR techniques. *Protein Sci.* 2, 543−558.

(39) Majumdar, A., Kettani, A., and Skripkin, E. (1999) Observation and measurement of internucleotide $^2J_{NN}$ coupling constants between ^{15}N nuclei with widely separated chemical shifts. *J. Biomol. NMR* 14, 67−70.

(40) Wishart, D. S., Bigam, C. G., Yao, J., Abildgaard, F., Dyson, H. J., Oldfield, E., Markley, J. L., and Sykes, B. D. (1995) ^{1}H, ^{13}C and ^{15}N

chemical shift referencing in biomolecular NMR. *J. Biomol. NMR* 6, 135−140.

(41) Delaglio, F., Grzesiek, S., Vuister, G. W., Zhu, G., Pfeifer, J., and Bax, A. (1995) NMRPipe: a multidimensional spectral processing system based on UNIX pipes. *J. Biomol. NMR* 6, 277−293.

(42) Goddard, T. D., and Kneller, D. G. (2006) *SPARKY 3*, University of California, San Francisco.

(43) Bax, A., Vuister, G. W., Grzesiek, S., Delaglio, F., Wang, A. C., Tschudin, R., and Zhu, G. (1994) Measurement of homo- and heteronuclear *J* couplings from quantitative *J* correlation. *Methods Enzymol.* 239, 79−105.

(44) Blomberg, F., Maurer, W., and Rueterjans, H. (1977) Nuclear magnetic resonance investigation of ^{15}N-labeled histidine in aqueous solution. *J. Am. Chem. Soc.* 99, 8149−8159.

(45) Tanokura, M. (1983) ^{1}H-NMR study on the tautomerism of the imidazole ring of histidine residues. I. Microscopic pK values and molar ratios of tautomers in histidine-containing peptides. *Biochim. Biophys. Acta, Protein Struct. Mol. Enzymol.* 742, 576−585.

(46) Roux-Fromy, M. (1982) On the Hill plot of NMR data for titration of proteins residues. *Biophys. Struct. Mech.* 8, 289−306.

(47) Vila, J. A. (2012) Limiting values of the ^{15}N chemical shift of the imidazole ring of histidine at high pH. *J. Phys. Chem. B* 116, 6665−6669.

(48) Boschcov, P., Seidel, W., Muradian, J., Tominaga, M., Paiva, A. C. M., and Juliano, L. (1983) Ionization constants and thermodynamic parameters of histidine and derivatives. *Bioorg. Chem.* 12, 34−44.

(49) Shimazaki, H., and Shinomoto, S. (2007) A method for selecting the bin size of a time histogram. *Neural Comput.* 19, 1503−1527.

(50) Pesce, A., Couture, M., Dewilde, S., Guertin, M., Yamauchi, K., Ascenzi, P., Moens, L., and Bolognesi, M. (2000) A novel two-over-two α-helical sandwich fold is characteristic of the truncated hemoglobin family. *EMBO J.* 19, 2424−2434.

(51) Majumdar, A., Kettani, A., Skripkin, E., and Patel, D. J. (1999) Observation of internucleotide NH···N hydrogen bonds in the absence of directly detectable protons. *J. Biomol. NMR* 15, 207−211.

(52) Reynolds, W. F., Peat, I. R., Freedman, M. H., and Lyerla, J. R., Jr. (1973) Determination of the tautomeric form of the imidazole ring of L-histidine in basic solution by carbon-13 magnetic resonance spectroscopy. *J. Am. Chem. Soc.* 95, 328−331.

(53) Vu, B. C., Vuletich, D. A., Kuriakose, S. A., Falzone, C. J., and Lecomte, J. T. J. (2004) Characterization of the heme-histidine cross-link in cyanobacterial hemoglobins from *Synechocystis* sp. PCC 6803 and *Synechococcus* sp. PCC 7002. *JBIC, J. Biol. Inorg. Chem.* 9, 183−194.

(54) Del Bene, J. E., and Bartlett, R. J. (2000) N-N spin-spin coupling constants [$^{2h}J(^{15}$N-^{15}N)] across N-H···N hydrogen bonds in neutral complexes: To what extent does the bonding at the nitrogens influence $^{2h}J_{N-N}$? *J. Am. Chem. Soc.* 122, 10480−10481.

(55) Sigala, P. A., Ruben, E. A., Liu, C. W., Piccoli, P. M., Hohenstein, E. G., Martinez, T. J., Schultz, A. J., and Herschlag, D. (2015) Determination of hydrogen bond structure in water versus aprotic environments to test the relationship between length and stability. *J. Am. Chem. Soc.* 137, 5730−5740.

(56) Witanowski, M., Webb, G. A., Stefaniak, L., Januszewski, H., and Grabowski, Z. (1972) Nitrogen-14 nuclear magnetic resonance of azoles and their benzo derivatives. *Tetrahedron* 28, 637−653.

(57) Roberts, J. D., Chun, Y., Flanagan, C., and Birdseye, T. R. (1982) A nitrogen-15 nuclear magnetic resonance study of the acid-base and tautomeric equilibria of 4-substituted imidazoles and its relevance to the catalytic mechanism of α-lytic protease. *J. Am. Chem. Soc.* 104, 3945−3949.

(58) Bachovchin, W. W., and Roberts, J. D. (1978) Nitrogen-15 nuclear magnetic resonance spectroscopy. State of histidine in catalytic triad of α-lytic protease. Implications for charge-relay mechanism of peptide-bond cleavage by serine proteases. *J. Am. Chem. Soc.* 100, 8041−8047.

(59) Bachovchin, W. W. (1986) ^{15}N NMR spectroscopy of hydrogen-bonding interactions in the active site of serine proteases:

evidence for a moving histidine mechanism. *Biochemistry 25*, 7751−7759.

(60) Schwarzinger, S., Kroon, G. J., Foss, T. R., Chung, J., Wright, P. E., and Dyson, H. J. (2001) Sequence-dependent correction of random coil NMR chemical shifts. *J. Am. Chem. Soc. 123*, 2970−2978.

(61) Benedict, H., Shenderovich, I. G., Malkina, O. L., Malkin, V. G., Denisov, G. S., Golubev, N. S., and Limbach, H. H. (2000) Nuclear scalar spin-spin couplings and geometries of hydrogen bonds. *J. Am. Chem. Soc. 122*, 1979−1988.

(62) Rosenberg, J. M., Seeman, N. C., Day, R. O., and Rich, A. (1976) RNA double-helical fragments at atomic resolution. II. The crystal structure of sodium guanylyl-3′,5′-cytidine nonahydrate. *J. Mol. Biol. 104*, 145−167.

(63) Seeman, N. C., Rosenberg, J. M., Suddath, F. L., Kim, J. J., and Rich, A. (1976) RNA double-helical fragments at atomic resolution. I. The crystal and molecular structure of sodium adenylyl-3′,5′-uridine hexahydrate. *J. Mol. Biol. 104*, 109−144.

(64) Alkorta, I., Elguero, J., and Denisov, G. S. (2008) A review with comprehensive data on experimental indirect scalar NMR spin-spin coupling constants across hydrogen bonds. *Magn. Reson. Chem. 46*, 599−624.

(65) Bloomfield, V. A., Crothers, D. M., and Tinoco, I. (2000) *Nucleic Acids: Structures, Properties, and Functions*, University Science Books, Sausalito, CA.

(66) Cocco, M. J., Kao, Y.-H., Phillips, A. T., and Lecomte, J. T. J. (1992) Structural comparison of apomyoglobin and metaquomyoglobin: pH titration of histidines by NMR spectroscopy. *Biochemistry 31*, 6481−6491.

(67) Banner, D. W., Bloomer, A., Petsko, G. A., Phillips, D. C., and Wilson, I. A. (1976) Atomic coordinates for triose phosphate isomerase from chicken muscle. *Biochem. Biophys. Res. Commun. 72*, 146−155.

(68) Lodi, P. J., and Knowles, J. R. (1991) Neutral imidazole is the electrophile in the reaction catalyzed by triosephosphate isomerase: structural origins and catalytic implications. *Biochemistry 30*, 6948−6956.

(69) Lodi, P. J., and Knowles, J. R. (1993) Direct evidence for the exploitation of an α-helix in the catalytic mechanism of triosephosphate isomerase. *Biochemistry 32*, 4338−4343.

(70) Drohat, A. C., Xiao, G., Tordova, M., Jagadeesh, J., Pankiewicz, K. W., Watanabe, K. A., Gilliland, G. L., and Stivers, J. T. (1999) Heteronuclear NMR and crystallographic studies of wild-type and H187Q *Escherichia coli* uracil DNA glycosylase: electrophilic catalysis of uracil expulsion by a neutral histidine 187. *Biochemistry 38*, 11876−11886.

(71) Drohat, A. C., Jagadeesh, J., Ferguson, E., and Stivers, J. T. (1999) Role of electrophilic and general base catalysis in the mechanism of *Escherichia coli* uracil DNA glycosylase. *Biochemistry 38*, 11866−11875.

(72) Cook, B. W., and Shaw, G. S. (2012) Architecture of the catalytic HPN motif is conserved in all E2 conjugating enzymes. *Biochem. J. 445*, 167−174.

(73) Wang, J., Tochio, N., Kawasaki, R., Tamari, Y., Xu, N., Uewaki, J. I., Utsunomiya-Tate, N., and Tate, S. I. (2015) Allosteric breakage of the hydrogen bond within the dual-histidine motif in the active site of human Pin1 PPIase. *Biochemistry 54*, 5242−5253.